Available online at www.sciencedirect.com
ScienceDirect
Journal of Power Sources 159 (2006) 987–994
JOURNAL OF POWER SOURCES
www.elsevier.com/locate/jpowsour

In situ simultaneous measurements of temperature and water partial pressure in a PEM fuel cell under steady state and dynamic cycling

S. Basu, M.W. Renfro *, H. Gorgun [1], B.M. Cetegen

Department of Mechanical Engineering, University of Connecticut, 191 Auditorium Road, U-3139, Storrs, CT 06269, United States

Received 12 October 2005; received in revised form 23 November 2005; accepted 25 November 2005
Available online 10 January 2006

Abstract

In situ, line-of-sight measurements of water vapor partial pressure and temperature were performed in a gas channel on the cathode side of an operating PEM fuel cell. Tunable diode laser absorption spectroscopy was employed for these measurements for which water transitions sensitive to temperature and partial pressure were utilized. The previously demonstrated methodology for water partial pressure measurements was extended to include temperature by including additional features of the water spectra in the data analysis. The combined technique was demonstrated in a PEM fuel cell operating under both steady state and time-varying load conditions. For steady state operation, the water partial pressure increases with increasing current density on the cathode side due to production of water by electrochemical reaction. Temperature in the gas phase remains relatively constant since the fuel cell housing temperature is controlled externally. For unsteady operation of the fuel cell through a time varying current profile, it is found that the water partial pressure responds to the load changes rapidly and follows the current profile. The gas temperature varies in response to the dynamic loading and departures from steady state conditions become more apparent at higher fuel cell operating temperatures.

Keywords: Fuel cell diagnostics; In situ measurements; Laser absorption spectroscopy; Water concentration; Temperature

1. Introduction

Proton exchange membrane (PEM) fuel cells generate electricity directly through two electrochemical reactions, which take place at the interface between a proton conductive membrane and catalyst electrodes. In a PEM fuel cell, controlled hydration of the membrane is required for proper operation. The hydrogen and oxygen feed streams are typically hydrated to bring water vapor into the cell, but several transport processes are responsible for nonhomogeneous distribution of water across the cell cross-section, including diffusion due to partial pressure gradients and electro-osmotic drag of water by protons through the membrane [1,2]. In addition, the cathode reactions produce water that may condense depending on local temperature and partial pressure. The fuel cell's overall performance can be very sensitive to water management since excessive water can lead to flooding and limit the rate of reactant transport to the electrodes and a reduction in water can decrease the protonic conductivity of the membrane. Nafion©, which is the most common membrane material exhibits a protonic conductivity change of an order of magnitude due to variation of relative humidity between 35 and 85% [3].

Similarly, the temperature of a PEM fuel cell impacts performance of the catalyst electrodes and impacts water transport and liquid/vapor balance. For these reasons, understanding of the distribution of water and local temperatures within operating fuel cells is important for optimizing system operation and design. Accurate, fast, in situ measurements of water concentration would enable both better understanding of water transport for improved cell design and advanced control strategies. In this paper, we describe an optical technique for simultaneously measuring water partial pressure and temperature in PEM cells based on water absorption of laser transmission through the flow passages in the bipolar plate. This approach permits non-intrusive in situ measurements and extends the capabilities of existing measurement techniques. The measurement approach is validated in steady state operation of a PEM cell with controlled humid-

* Corresponding author. Tel.: +1 860 486 5934; fax: +1 860 486 5088.
E-mail address: renfro@engr.uconn.edu (M.W. Renfro).
[1] Present address: Yildiz Technical University, Istanbul, Turkey.

0378-7753/$ – see front matter © 2005 Elsevier B.V. All rights reserved.
doi:10.1016/j.jpowsour.2005.11.091

ity of incoming gas streams and cell temperature. The optical measurement is then applied to the PEM cell undergoing cyclic loading to simulate the conditions that might be present in transportation applications where instantaneous power requirements fluctuate. The measurements of water partial pressure and temperature in the cathode flow passages detail the time response of the system to transient events.

2. Background

Development of tools for sensing of temperature and chemical species in fuel cells is a relatively new area of research. Prior to the last 5 years, most measurements in fuel cell systems were limited to global measurements of electrical cell performance. Polarization curve measurements, for example, are routinely used to track cell performance and can be combined with simple models to diagnose component problems in the cell [4]. More recent refinement of global measurement techniques has permitted monitoring of flooding or drying conditions based on pressure drop across the cell [5,6], separation of anode and cathode contributions to cell polarization based on impedance spectroscopy [7], and diagnosis of gas diffusivities at electrodes based on rapid gas supply interruption [8]. However, these techniques are generally limited to providing only information integrated across the cell.

More recent developments have enabled characterization of local cell conditions. The development of segmented fuel cells enabled measurements of local electrical performance [9,10]. Observation of local chemical conditions have been made using simple visual observations of bubble formation through windowed direct methanol fuel cells [11], physical probe measurements using gas chromatography [12,13], and more sophisticated optical approaches such as liquid water measurements via neutron scattering [14,15], membrane hydration via X-ray scattering [16], catalyst composition via X-ray absorption [17,18], Fourier transform infrared (FT-IR) spectroscopy [19], and membrane water content and acidity via fiber-based fluorescence [20,21].

Of the techniques available for local measurements of chemical composition, most are limited by either requiring extractive sampling as in the case of gas chromatography and FT-IR spectroscopy, which limits their temporal response, or by using facilities that are not easily implemented in routine system measurements, as in the case of neutron scattering and X-ray absorption. Consequently, Basu et al. [22,23] recently developed an in situ non-intrusive method of monitoring water vapor partial pressure in each of the gas distribution channels in the bipolar plate of a PEM fuel cell using tunable diode laser absorption spectroscopy (TDLAS). This technique provided the first water vapor measurements without using physical probes in active fuel cells. However, the diode laser system used by Basu et al. [22] was not able to resolve the temperature variation in the PEM fuel cell due to the temperature insensitivity of the water absorption profiles at the chosen laser wavelength. In the current work, the TDLAS system has been modified by altering the laser wavelength to access multiple water transitions with different temperature sensitivities, enabling simultaneous recovery of both water vapor partial pressure and gas-phase temperature. The improved system has sufficient temporal resolution to examine the variations in gas-phase composition and temperature in a single localized flow passage of the bipolar plate during unsteady fuel cell operation. Results are reported for a fuel cell running under both steady and dynamic conditions simulating the nonuniform loading that might occur in real life transportation applications.

In the following sections, the theoretical and experimental approaches taken for water vapor concentration and temperature measurements are first described. Results on the application of the measurement technique to a laboratory scale PEM fuel cell are subsequently presented.

3. Experimental approach

The experimental methodology is based on that reported by Basu et al. [22]. Tunable diode laser absorption spectroscopy was used to measure water vapor absorption profiles as a function of excitation wavelength. However, the laser was changed from the previous experiments to enable measurement of water transitions in a different wavelength regime. In this work, the fiber pig-tailed output of a distributed feedback (DFB) diode laser (NEL # NLK1S5G1AA) at a wavelength of 1470 nm in the near-IR range was split using a 2×2 fiber splitter. One leg of the splitter was directly coupled to a photodiode as a reference measurement of the laser power without water absorption (I_0). The output from the other leg was passed through an optically accessible PEM fuel cell using a modified bipolar plate described by Basu et al. [22]. The bipolar plate had a serpentine geometry so that long flow passages extended over the entire fuel cell width [22]. The bipolar plate contained 17 channels of which the third channel from the air inlet on the cathode side was milled out to the end of the bipolar plate and fitted with miniature collimating optics so that the laser emission could pass through the cell. However, the diagnostic technique works equally well for all channels and could be extended to multiple channel monitoring by multiplexing. In this configuration, the total absorption path length is 7 cm. Since the measurement technique for determining water partial pressure is linear, the measurement recovers the path averaged value of partial pressure. With the current setup, variations along the line-of-sight cannot be determined. In previous work, these passages were sealed with small windows at the end of the passage and the laser was collimated externally. The alignment of this system was tedious since the length to width ratio of the channel is approximately 100. For these new experiments, our previous bipolar plate was modified by placing small collimating lenses, coupled with the optical fibers, directly in the ends of the flow passages, which served to both seal the flow passage and collimate the laser beam. The fiber output from the laser was then placed directly in the fuel cell improving the repeatability of laser alignment.

The laser output was captured using an identical photodiode as for the reference channel and measured the attenuated laser power through the cell including absorption from water

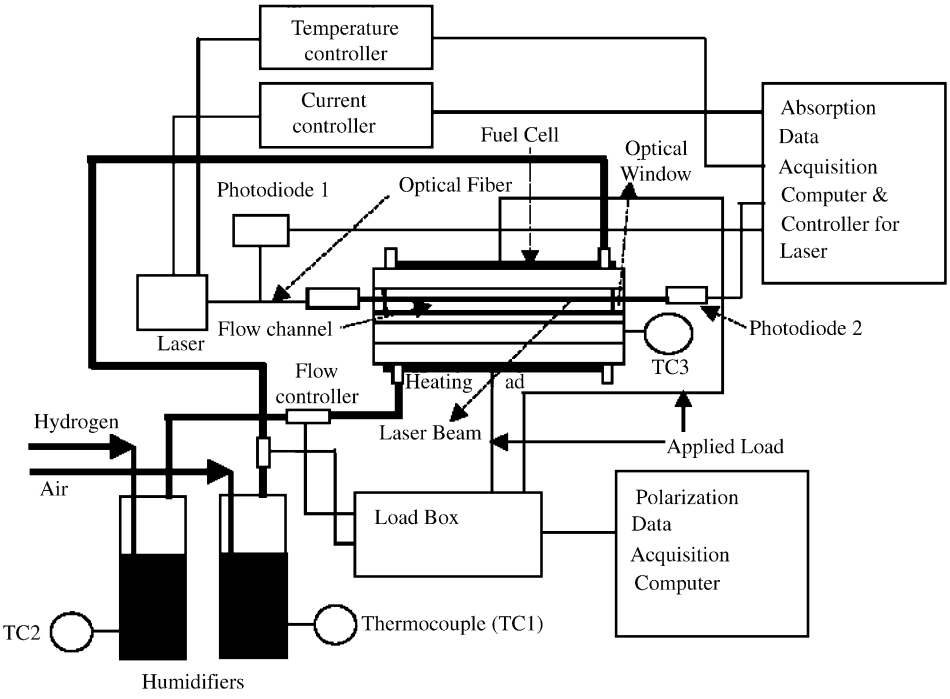

Fig. 1. Experimental setup for calibration, steady state, and dynamic tests. Numerous thermocouples (TC) were used to control the humidity of the cell.

and non-resonant losses (I). The hydrogen and air streams fed to the fuel cell were humidified by passing them through a temperature controlled water bath to saturate the streams, as shown in Fig. 1. Further heating of the gases, and electrical heating pads on the fuel cell surface were used to provide independent control of gas and fuel cell temperatures and gas humidities. The external electrical load on the fuel cell was controlled by a Scribner 890CL fuel cell test system load box. For calibration of the new laser system, the cell was fed with heated moist air of known relative humidity but was not fed with hydrogen or electrically loaded so that there was no electrochemical reaction to alter the relative humidity of the cell. Dry to fully saturated conditions could be achieved for temperatures from 60 to 85 °C, in the range of interest for PEM fuel cells. The pressure in the cell was atmospheric for all cases reported here.

The absorption of the laser beam passing through the gas sample is related to the partial pressure, P_s (atm), of the absorbing species by Beer's law [24]:

$$\frac{I}{I_0} = \exp\left(-\int_0^L \kappa P_s \, dl\right) \quad (1)$$

where κ (atm^{-1} cm^{-1}) is the wavelength and temperature dependent absorption coefficient. The integration is performed over the path length L of the gas sample through the bipolar plate. The absorption coefficient displays strong peaks as a function of wavelength due to the discrete rotational and vibrational energy transitions of molecular species. The absorption coefficient is also temperature dependent since the distribution of water molecules among its various energy levels and the width of each transition depend on temperature. Theoretical predictions of these variations are discussed in the next section.

The DFB laser used here has a spectral bandwidth that is much narrower than the molecular transitions. The laser's wavelength depends on both the laser temperature and the current used to drive the diode laser. An imbedded thermoelectric cooler in the laser and a Thorlabs TEC2000 temperature controller were used to control the laser temperature and permit coarse tuning of the laser wavelength over its range. However, during measurements, the temperature was held constant. A Thorlabs LDC5000 current controller was used for rapid variation of the laser wavelength by altering the current injection into the diode laser. The laser current was modulated with a 500 Hz ramp function generated with a data acquisition computer. This ramp modulation alters the power as well as the wavelength of laser emission. The laser wavelength can be varied over 0.15 nm and scanned through water absorption features. The reference photodiode directly monitors the laser power prior to entering the fuel cell to account for its variation with injection current. The peak laser absorption was typically around 2% for the conditions examined. Thus, the water absorption features appear as small dips in the measured laser intensity emerging from the test cell [22]. By taking the ratio of the laser intensity before and after the test cell (I/I_0), the relative absorption is determined as a function of time. An example of the measured absorption spectrum for the new laser is shown in Fig. 2.

The laser wavelength as a function of temperature and current was calibrated using an optical spectrum analyzer. Data from the photodiodes were acquired at rate of 500 kHz collecting 1000 samples for each current scan resulting in a scan time of 2 ms. Typically, 500 scans were averaged to obtain absorption data, which were then processed to determine the water vapor partial pressure and temperature as described in the next section.

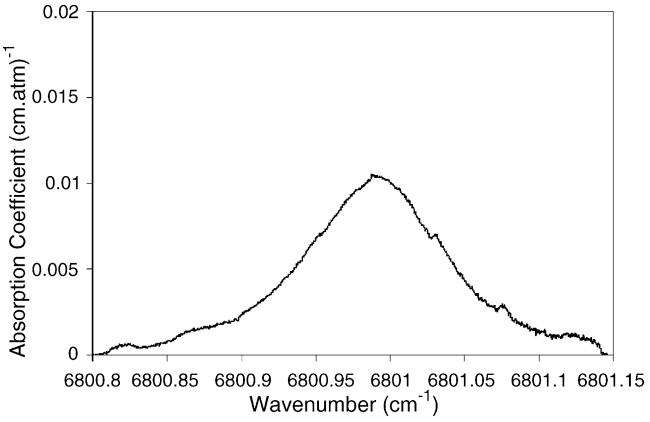

Fig. 2. Sample spectrum measured in fuel cell using tunable diode laser absorption spectroscopy. The local maximum at 6801 cm^{-1} is the strong water transition used for the measurements in this work.

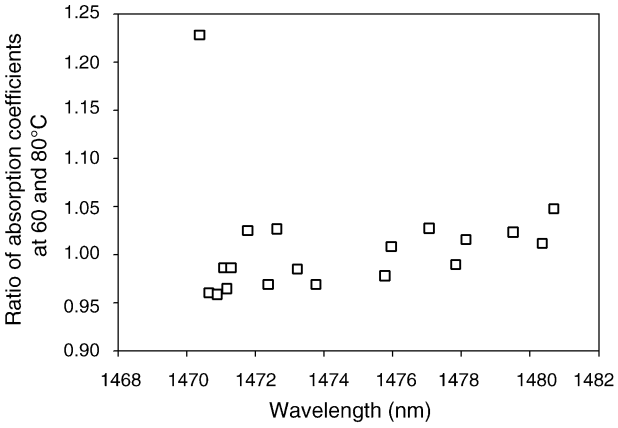

Fig. 3. Ratio of absorption coefficients at 60 and 80 °C vs. line center wavelength.

4. Spectral simulations

The experimental study reported by Basu et al. [22] showed that the ro-vibrational transitions available at 1491 nm, which was the wavelength of the laser used in that study, were not sufficiently sensitive to temperature in the range from 60 to 90 °C. The absorption intensity varied by only 10% and the spectral width varied by only 2.2% and did not allow extracting temperature in addition to water partial pressure. Thus, for the current work a more exhaustive analysis of the water spectrum from 1400 to 1650 nm was carried out to determine transitions that may be suitable for temperature measurements in the range of interest to PEM cells. The range of 1400–1650 nm was chosen since commercially available, relatively inexpensive diode lasers are manufactured in this range.

A simulation of water absorption spectra using the HITRAN database [25] was executed over the range of 1400–1650 nm at typical PEM conditions of water partial pressure equal to 0.19 atm and temperatures of 60–80 °C. The ro-vibrational transitions of water vapor were simulated using a Voigt function convolution with the HITRAN intensity and width data. It was found in our previous experiments that absorption coefficients greater than 0.0035 cm^{-1} atm^{-1} could be accurately measured with direct absorption in the PEM cell. Thus, an intensity cutoff was introduced in the code to filter out spectral lines with absorption coefficients below 0.0035 cm^{-1} atm^{-1}. The purpose of this exercise was to extract absorption coefficients, which are accurately measurable, and to ascertain their temperature sensitivity.

The simulated absorption coefficients at temperatures of 60 and 80 °C were divided by one another to determine the relative change in absorption with temperature only at fixed partial pressure. Fig. 3 illustrates these results for all transitions meeting the threshold absorptivity requirement at wavelengths between 1468 and 1482 nm (a subset of the entire range examined). The transition near 1470 nm shows a 23% variation of peak absorption coefficient with temperature, which is the greatest temperature sensitivity of all lines examined. All the other transitions in the wavelength range of 1400–1650 nm have temperature sensitivities much less than 20%. The NEL laser (NLK1S5G1AA) was thus selected for measurements in this region.

An experimental methodology for extracting partial pressure and temperature simultaneously was developed based on the HITRAN [25] simulations. Fig. 4 illustrates the simulated absorption profiles in the range 1470.30–1470.42 nm (6800.75–6801.3 cm^{-1}) across the temperature sensitive water feature for a fixed temperature of 80 °C with different water partial pressures. As explained by Basu et al. [22], water–water collisions are very effective at broadening the water absorption profiles (compared to water–air collisions); thus, the width of the profile changes substantially with water partial pressure. In fact, the increase in profile width is so strong that the peak intensity of the water absorption actually decreases with increasing water partial pressure. Since the temperature remains constant, this halfwidth change is dominated by the Lorentzian part of the Voigt profile, which governs collisional broadening. Consistent with our previous work, a Lorentzian profile can be used in place of the more complicated Voigt profile to describe the profile shape with minimal error [22]. For this transition, the width varies by 60% for water partial pressure variations of 0.19–0.45 atm.

Fig. 5 shows simulated normalized water spectra for the coldest and hottest conditions expected in the PEM fuel cell at the

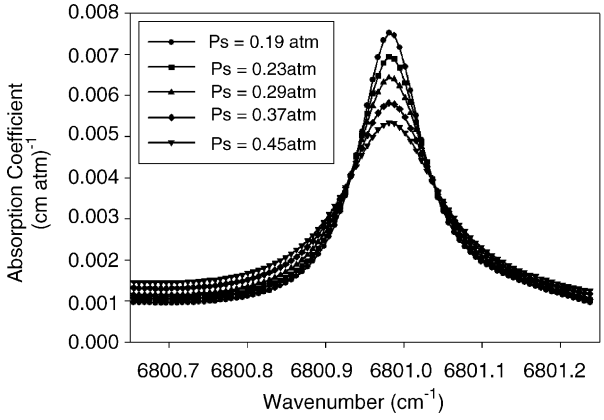

Fig. 4. Simulated absorption profiles for different partial pressures at $T = 80$ °C.

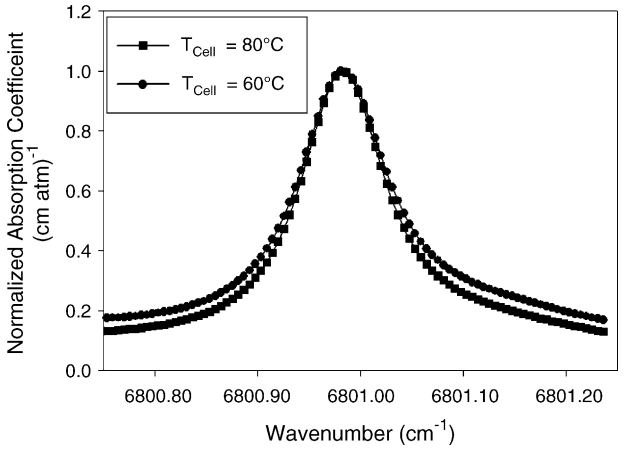

Fig. 5. Normalized absorption profiles at 60 and 80 °C for $P_s = 0.19$ atm.

same partial pressure of 0.19 atm. The absorption peaks vary by about 23% for a change of temperature of 20 °C, but there is less than 5% change in the profile width, which is dominated by collisional broadening of water–water collisions as is evident from Fig. 5. These observations suggest that the width and intensity of measured profiles can be used to extract simultaneously water partial pressure and temperature. This was not possible in our previous work since the laser wavelength available probed a temperature insensitive water transition.

Figs. 6 and 7 illustrate these results in detail, where the predicted profile halfwidths are shown for five separate transitions that are each accessible with the NEL laser acquired for these measurements. The variation with temperature (Fig. 6) is very small in each case, while the variation with partial pressure (Fig. 7) is significant. Thus, a curve fit to the measured data similar to that described by Basu et al. [22] can extract the partial pressure independent of temperature from the halfwidth. Since the peak intensity is both a function of partial pressure and temperature, knowledge of the partial pressure can then be used to extract the temperature from the peak intensity. Fig. 8 shows the variation of peak absorption coefficient with temperature for various partial pressure conditions based on the HITRAN simulations. Once the partial pressure is obtained from the halfwidth, a constant partial pressure line is chosen and the peak absorption

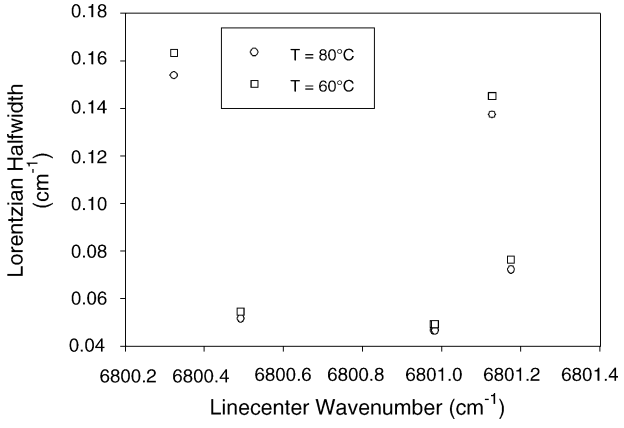

Fig. 6. Variation of Lorentzian halfwidth with temperature.

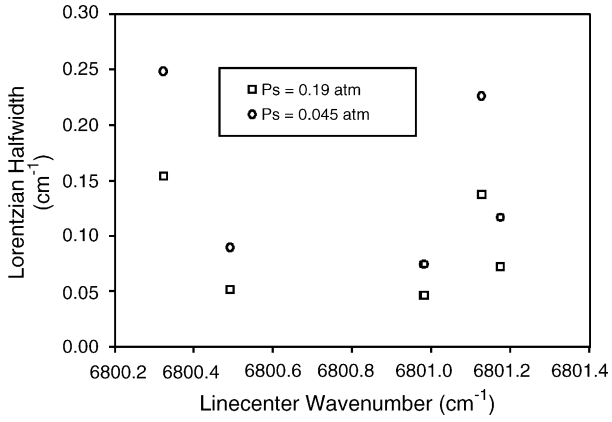

Fig. 7. Variation of Lorentzian halfwidth with partial pressure at $T = 80$ °C.

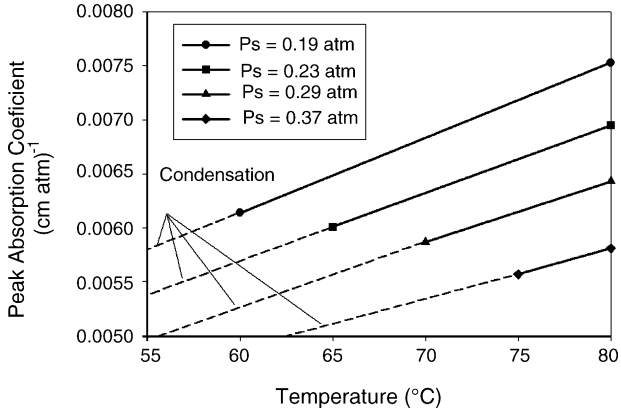

Fig. 8. Variation of peak absorption coefficients with temperature for different partial pressure conditions.

coefficient is related to the temperature. The dashed lines indicate the zone where the water becomes saturated at the predicted temperature so that two-phase flow would exist in the bipolar plate. No experimental data in this zone is possible since condensation inside the gas channels prevent transmission of the laser beam. In fact, the loss of absorption signal is a good indicator of water condensation in the flow channel as a result of beam path blockage. The spacing between the iso-partial pressure lines is sufficient for an accurate determination of both temperature and water vapor partial pressure as demonstrated in the experimental measurements described in this paper. Since these measurements are based on equilibration of rotational molecular energy modes, which are much faster than the dynamic processes occurring in fuel cells, this technique is applicable for steady state and dynamic operation of the fuel cell.

5. Experimental results

5.1. System calibration

Measurements were first made in the fuel cell without external loading or hydrogen flow to calibrate the measured halfwidths and spectral intensities against the simulations presented in the previous section. As established from the HITRAN simulation, the experimental profiles are predomi-

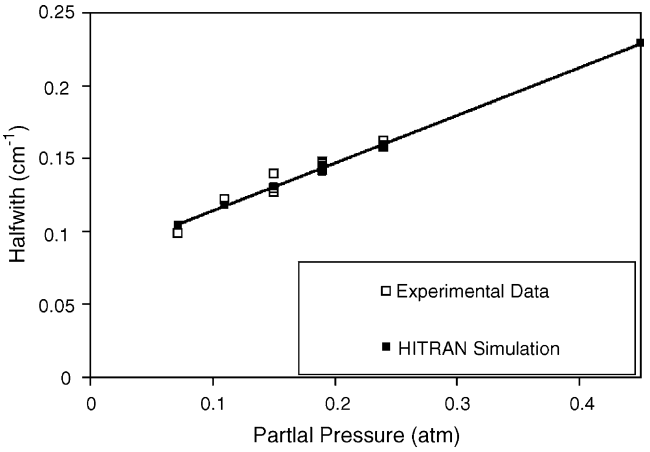

Fig. 9. Halfwidth calibration vs. partial pressure.

nately Lorentzian and in the spectral window available with the current laser, five water transitions contribute significantly to the overall absorption shape. The data analysis procedure consists of fitting five Lorentzian profile shapes over the experimental data, similar to previous curve fits in a different spectral range [26]. The line central wavelengths of the five Lorentzians were taken from the HITRAN database and only the widths and peak intensities of the five Lorentzians were varied. In addition, a third order polynomial curve fit to the slowly varying background was included. The halfwidth and intensity of the primary transition of interest at 6801 cm^{-1} was then used for further analysis. Fig. 9 shows the measured and simulated profile halfwidths for this line versus partial pressure. In the calibration experiments, the temperature and partial pressure are known since they are externally controlled. There is good agreement between the theoretical halfwidth versus partial pressure and experimental counterpart within 10% over a wide range of partial pressure values. Fig. 10 shows the measured peak intensities as a function of water partial pressure and temperature, both controlled in the calibration experiments. The peak intensity is related to temperature linearly and separate calibration lines for each partial pressure are found as predicted in Fig. 8. The shift in peak intensity at a fixed temperature with variation of partial pressure is due to line broadening as shown in Fig. 4. This calibration diagram is subsequently used in the active fuel cell measurements to determine the temperature once the partial pressure of water is known from the measurements of Fig. 9.

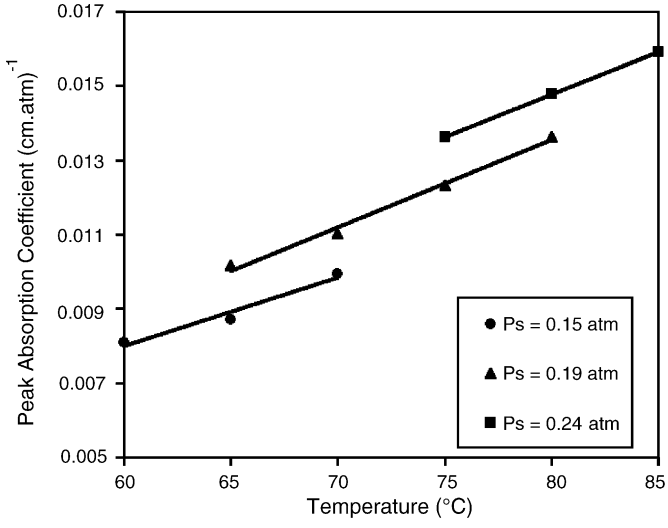

Fig. 10. Calibration of peak intensities.

5.2. Results from steady state fuel cell tests

Measurements of water partial pressure and temperature were carried out on the air (cathode) side of the fuel cell. The operating temperature of the fuel cell was varied over the range from 60 to 80 °C. The relative humidity of the air and H_2 entering the cathode and anode sides of the fuel cell was also varied from 40 to 90%. The flow rate of air was maintained at 1.2 lpm while that of hydrogen was fixed at 1.0 lpm for all the measurements reported here. The external load was varied as a step function so that each load setting corresponds to a particular value of the current density drawn from the cell. Spectroscopic measurements were carried out at each value of the load after allowing the cell to reach steady state operation. Fig. 11 illustrates the water partial pressures and temperatures obtained under these conditions using the calibration curves of Figs. 9 and 10. The water vapor partial pressure rises from the inlet value as more current is drawn from the cell. As the load on the fuel cell increases, the current and therefore the proton flux also increases. This increased current produces more water at the cathode side and

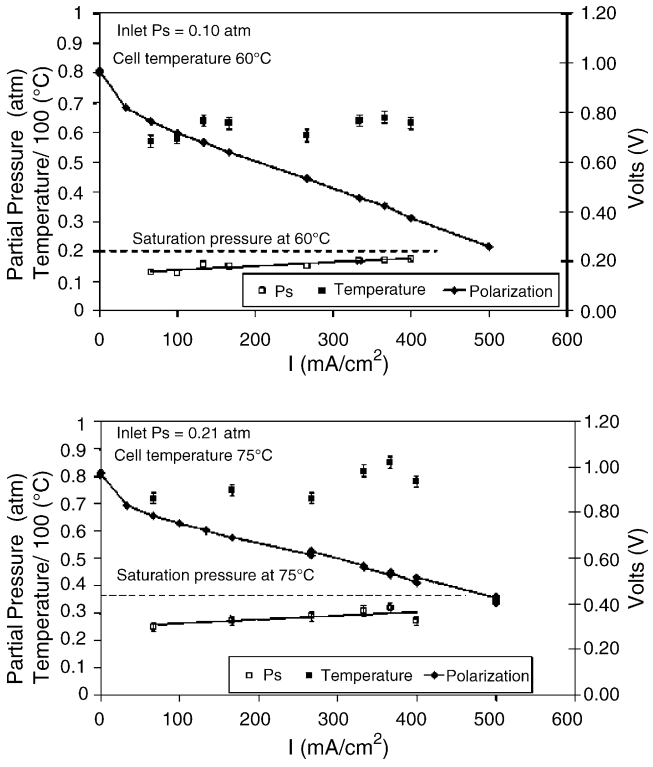

Fig. 11. Partial pressure and temperature measurements under steady state operation at 60 °C (P_{sat} = 0.20 atm) and 75 °C (P_{sat} = 0.38 atm).

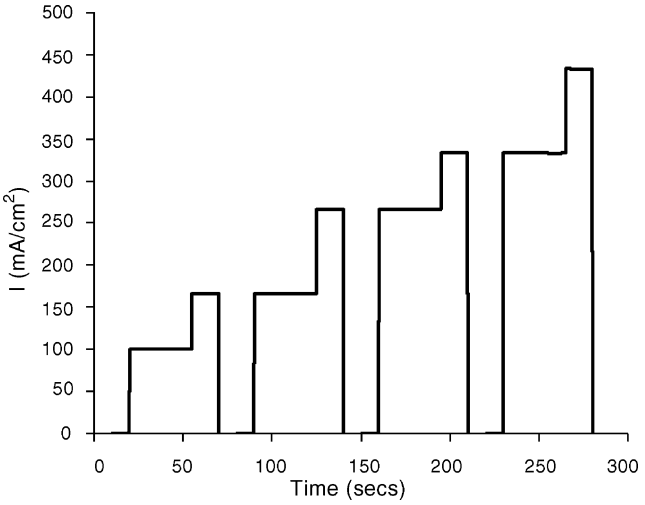

Fig. 12. Sample dynamic cycle.

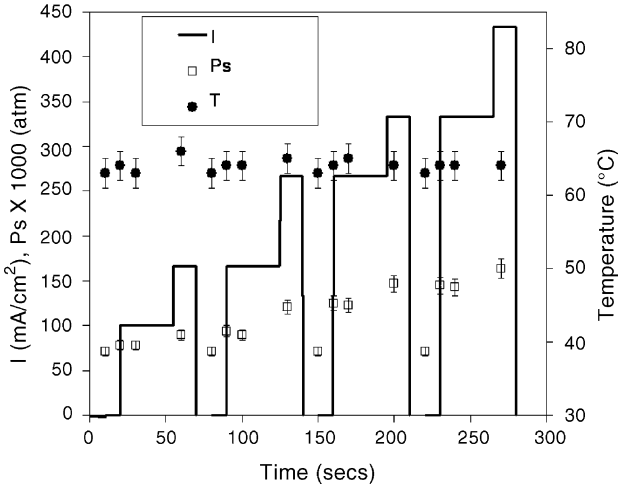

Fig. 13. Partial pressure and temperature measurements for inlet $P_s = 0.07$ atm, cell temperature = 60 °C ($P_{sat} = 0.20$ atm) with dynamic cycling.

results in the increased water partial pressure observed. All the experimental data collected show a similar increase in partial pressure with current density similar to the work reported by Basu et al. [22]. Since the temperature of the cell is controlled by an external heating pad and is allowed to reach steady state for each operating condition, the steady state temperature profiles do not show significant changes as the current is increased for low currents. At higher currents, the heat production in the cell is large enough to show a 5–10 °C rise in the local gas-phase temperature.

An error estimate of the results is obtained from the calibration curve for partial pressure in Fig. 9, where the scatter of the data points about the linear fit is about ±5% similar to our measurements with a different laser system [22]. The error in the temperature measurement, arises from three sources: (1) measurement noise seen as scatter of the experimental data points about the linear best fit of Fig. 10, (2) error from the linear interpolation of the temperature if the value of the peak intensity falls in between two calibrated pressure lines, and (3) the ±5% uncertainty in the measurement of the partial pressure, which in turn results in an uncertainty in locating the iso-partial pressure line for temperature determination. All these sources of error combined results in an uncertainty of ±2.5 °C in temperature determination from the measured data.

5.3. Results from dynamic conditions

In addition to temperature recovery, a novel aspect of the current work is the extension of measurements of fuel cell gas-phase properties to fuel cells undergoing dynamic cycling, which is of importance to the automobile industry. Transient gas-phase measurements using non-intrusive laser-based in situ diagnostics during a dynamic cycle have not been reported, to our knowledge. The experimental procedure is the same as described in previous sections, except that the external load on the cell is varied according to the load schedule recommended by the US Fuel Cell Council [27]. The external load sequence, shown in Fig. 12, has a total cycle time of 300 s.

Measurements of water absorption spectra and the resulting partial pressures and temperatures were measured just before, during the rise, and near the end of each dynamic feature in the load cycle. Fig. 13 shows the partial pressure and temperature profiles for a fuel cell operating under this dynamic cycle with the nominal cell temperature of 60 °C and inlet water vapor partial pressure in the air stream of 0.07 atm. For these conditions, the cell temperature does not show significant variation. However, the water partial pressure is observed to increase during each dynamic load feature as more current is drawn. The water partial pressures measured immediately after the fast rise in each feature are identical to those measured 10 s later, indicating that the gas composition follows the electrical loading very rapidly. Likewise, after each load is removed rapidly, the water partial pressure returns to the inlet value within 10 s. These measurements show that the time response of the cell is significantly less than 10 s to follow these rapid changes.

Fig. 14 shows similar measurements during the same load cycle but with a nominal cell temperature of 80 °C and an inlet water partial pressure of 0.19 atm. The dashed line in Fig. 14

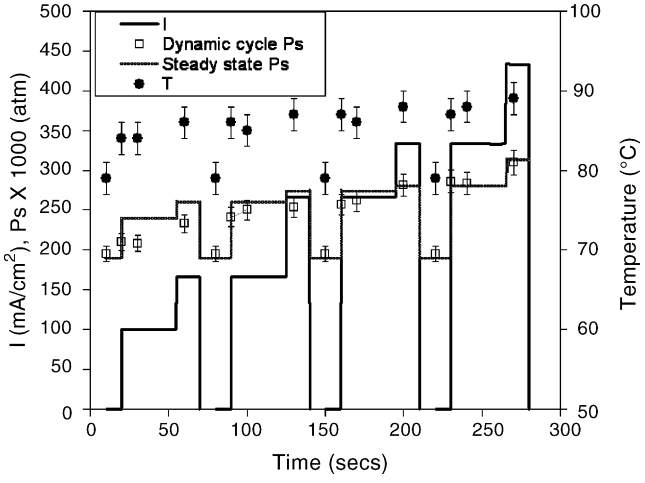

Fig. 14. Partial pressure and temperature measurements for inlet $P_s = 0.19$ atm, cell temperature = 80 °C ($P_{sat} = 0.47$ atm) with dynamic cycling.

represents the values of water partial pressure that would be obtained under steady state conditions with the same cell temperature and current based on the measurements of Fig. 11. The quasi-steady state values are slightly higher than the values measured under dynamic cycling for low currents. During the last half of the dynamic load cycle, when the peak current is higher, the actual and quasi-steady values are equal within the uncertainty. Thus, the fuel cell reaches a value closer to quasi-steady conditions when cycling to higher currents. As with the colder cell measurements, the measurements made 10 s after the fast fall features in the cycle have attained the inlet partial pressure values. Thus, for both operating conditions, the time response of the gas-phase properties are less than 10 s, and in fact must be much less than 10 s to achieve complete equilibration when the cell is unloaded. It should be noted that the measurements reported here are spatially averaged across the channel length with a temporal resolution of about 8 s; thus, local and temporal variations from these results with finer resolution cannot be excluded.

With the hotter fuel cell operating conditions, the cell temperature noticeably rises during each load cycle feature, as shown in Fig. 14. While the cell is nominally controlled at 80 °C, the local temperature in the gas passage of the bipolar plate rises as high as 90 °C due to the rapid cycling of the cell from the steady state value. The external temperature control cannot follow these rapid changes. The temperature is controlled by a temperature controller whose response time and the time needed for heat to dissipate and make the cell attain the nominal value is large compared to the cell cycling time. Partial pressure on the contrary is not controlled by external means. For partial pressure, it is the chemical kinetics, which is responsible for adjusting to the dynamic cycling of the external load. Fig. 14 suggests that the chemical kinetics and water transport is fast enough to reach nearly quasi-steady conditions.

6. Conclusions

The measurement of partial pressure and temperature during steady state and dynamic cycle operation of a PEM fuel cell was demonstrated with a novel diagnostic technique by monitoring laser transmission and water absorption through a flow passage in the bipolar plate. Simulations of water absorptivity were utilized to select a laser wavelength that optimized sensitivity to temperature and partial pressure for conditions relevant to a PEM fuel cell. Calibration measurements in a non-operating cell were used to validate the model. The new laser system was applied to measurements in a steady state cell, similar to previous work [22], and was extended to include temperature measurements and measurements of both temperature and water partial pressure during dynamic fuel cell operation simulating conditions that may occur in automotive applications where power demand fluctuates. The non-intrusive in situ measurements do not disturb the fuel cell operation and indicate that the gas-phase properties follow the external loading with a time response of less than 10 s. However, the internal temperature in the flow passages of the bipolar plate are not fully regulated by external fuel cell heating pads and show significant 10 °C increase during dynamic fuel cell operation.

Acknowledgments

The research reported here was funded by the U.S. Army RDECOM, CERDEC (Fort Belvoir, VA) through the Connecticut Global Fuel Cell Center (CGFCC). The authors would like to acknowledge the useful discussions with Dr. Frano Barbir over the course of this work.

References

[1] J. Larminie, A. Dicks, Fuel Cell Systems Explained, Wiley, New York, 2000.
[2] P. Costamagna, S. Sirinivasan, J. Power Sources 102 (2001) 253–269.
[3] G. Alberti, M. Casciola, L. Massinelli, B. Bauer, J. Membr. Sci. 185 (2001) 73–81.
[4] M.L. Perry, J. Newman, E.J. Cairns, J. Electrochem. Soc. 145 (1998) 5–15.
[5] F. Barbir, H. Gorgun, X. Wang, J. Power Sources 141 (2005) 96–101.
[6] W.S. He, G.Y. Lin, T. Van Nguyen, AIChE J. 49 (2003) 3221–3228.
[7] J.T. Mueller, P.M. Urban, J. Power Sources 75 (1998) 139–143.
[8] J. Stumper, H. Haas, A. Granados, J. Electrochem. Soc. 152 (2005) A837–A844.
[9] J. Stumper, S.A. Campbell, D.P. Wilkinson, M.C. Johnson, M. Davis, Electrochem. Acta 43 (1998) 3773–3783.
[10] M.M. Mench, C.Y. Wang, M. Ishikawa, J. Electrochem. Soc. 150 (2003) A1052–A1059.
[11] H. Yang, T.S. Zhao, Q. Ye, J. Power Sources 139 (2005) 79–90.
[12] Q. Dong, J. Kull, M.M. Mench, J. Power Sources 139 (2005) 106–114.
[13] M.M. Mench, Q.L. Dong, C.Y. Wang, J. Power Sources 124 (2003) 90–98.
[14] D. Kramer, J. Zhang, R. Shimoi, E. Lehmann, A. Wokaun, K. Shinohara, G.G. Scherer, Electrochem. Acta 50 (2005) 2603–2614.
[15] R. Satija, D.L. Jacobson, M. Arif, S.A. Werner, J. Power Sources 129 (2004) 238–245.
[16] V.R. Albertini, B. Paci, A. Generosi, S. Panero, M.A. Navarra, M. di Michiel, Electrochem. Solid State Lett. 7 (2005) A519–A521.
[17] R. Viswanathan, R. Liu, E.S. Smotkin, Rev. Sci. Instrum. 73 (2002) 2124–2127.
[18] A.E. Russell, S. Maniguet, R.J. Mathew, J. Yao, M.A. Roberts, D. Thompsett, J. Power Sources 96 (2001) 226–232.
[19] I. Tkach, A. Panchenko, T. Kaz, V. Gogel, K.A. Friedrich, E. Roduner, Phys. Chem. Chem. Phys. 6 (2004) 5419–5426.
[20] Y.P. Patil, T.A.P. Seery, M.T. Shaw, R.S. Parnas, ACS Fuel Chem. Pre. 49 (2004) 683.
[21] Y.P. Patil, T.A.P. Seery, M.T. Shaw, R.S. Parnas, Ind. Eng. Chem. Res. 44 (2005) 6141.
[22] S. Basu, H. Xu, M.W. Renfro, B.M. Cetegen, ASME J. Fuel Cell Sci. Tech. 3 (2006).
[23] S. Basu, In situ optical diagnostics in a PEM fuel cell using near IR absorption spectroscopy, M.S. Thesis, University of Connecticut, 2004.
[24] S.S. Penner, Quantitative Molecular Spectroscopy and Gas Emissivities, Addison-Wesley, 1959.
[25] L.S. Rothman, C.P. Rinsland, A. Goldman, S.T. Massie, E.D.P. Edwards, J.M. Flaud, A. Perrin, C. Camy-Peyret, V. Dana, J.Y. Mandin, J. Schroeder, A. McCann, R.R. Gamache, R.B. Wattson, K. Yoshino, K.V. Chance, K.W. Jucks, L.R. Brown, V. Nemtchinov, P. Varanasi, J. Quant. Spectrosc. Radiat. Trans. 60 (1998) 665–710.
[26] B.H. Armstrong, J. Quant. Spectrosc. Radiat. Trans. 7 (1966) 61–68.
[27] US Fuel Cell Council, Protocol on Fuel Cell Component Testing, 2005, http://www.usfcc.com.